

SYNTHESIS AND CHARACTERIZATION OF VISIBLE-LIGHT-DRIVEN PHOTOCATALYSIS OF RHODAMINE B BY HETEROJUNCTION $\text{Ag}_3\text{VO}_4/\text{Bi}_2\text{WO}_6$ NANOCOMPOSITES

A. PHURUANGRAT^{a,*}, B. KUNTALUE^b, P. PATIPHATPANYA^c,
N. EKTHAMMATHAT^d, P. DUMRONGROJTHANATH^e,
S. THONGTEM^{f,g}, T. THONGTEM^{c,g}

^a*Department of Materials Science and Technology, Faculty of Science, Prince of Songkla University, Hat Yai, Songkhla 90112, Thailand*

^b*Electron Microscopy Research and Service Center, Faculty of Science, Chiang Mai University, Chiang Mai 50200, Thailand*

^c*Department of Chemistry, Faculty of Science, Chiang Mai University, Chiang Mai 50200, Thailand*

^d*Program in Chemistry, Faculty of Science and Technology, Bansomdejchaopraya Rajabhat University, Bangkok 10600, Thailand*

^e*Rajamangala University of Technology Lanna Chiang Rai, Chiang Rai 57120, Thailand*

^f*Department of Physics and Materials Science, Faculty of Science, Chiang Mai University, Chiang Mai 50200, Thailand*

^g*Materials Science Research Center, Faculty of Science, Chiang Mai University, Chiang Mai 50200, Thailand*

Visible-light-driven $\text{Ag}_3\text{VO}_4/\text{Bi}_2\text{WO}_6$ photocatalysts with different weight contents of Ag_3VO_4 used for degradation of rhodamine B (RhB) were successfully synthesized by a deposition-precipitation method. The as-prepared pure Bi_2WO_6 sample and heterostructure $\text{Ag}_3\text{VO}_4/\text{Bi}_2\text{WO}_6$ nanocomposites were analyzed by X-ray diffraction (XRD), scanning electron microscopy (SEM), transmission electron microscopy (TEM), high resolution transmission electron microscopy (HRTEM) and selected area electron diffraction (SAED). In this research, the Ag_3VO_4 nanoparticles were supported on thick Bi_2WO_6 nanoplates. The heterostructure 10 wt% $\text{Ag}_3\text{VO}_4/\text{Bi}_2\text{WO}_6$ nanocomposites showed the highest photocatalytic performance for RhB degradation of 95% under visible light irradiation within 80 min due to the separation of photo-excited charge carriers and inhibition of photo-induced electron-hole pairs.

(Received August 25, 2019; Accepted December 4, 2019)

Keywords: $\text{Ag}_3\text{VO}_4/\text{Bi}_2\text{WO}_6$ nanocomposites; Photocatalysis; Electron microscopy; Spectroscopy

1. Introduction

The photocatalytic splitting of water and the photodegradation of organic compound by TiO_2 have been intensively investigated in recent years because of its low cost, high efficiency and good stability. Nevertheless, it is active only under UV light irradiation with ~4% of the solar energy and shows rapid recombination of photogenerated charge carriers [1–3]. For the visible light with ~43% of the solar energy, visible-light-driven photocatalytic semiconductor has been tremendously developed for oxidization of organic pollutant containing in water and air and for hydrogen generation [1, 2].

Bismuth tungstate (Bi_2WO_6) with band gap of ~2.7 eV is an excellent visible-light-driven photocatalytic semiconductor for organic pollutant oxidization and hydrogen generation because it

* Corresponding authors: phuruangrat@hotmail.com

is non-toxic, chemical stability, thermal stability and eco-friendliness [4–7]. The superior properties of Bi_2WO_6 can be ascribed to its stacking layer structure of WO_6 octahedron and $(\text{Bi}_2\text{O}_2)^{2+}$ layers which can promote the separation of photo-generated charges and can capture the inter-layer water molecules to delay photogenerated charge carrier recombination [3, 4, 8, 9]. However, Bi_2WO_6 is still needed for further improvement of its photocatalytic performance because it has narrow light-absorption range, high rate of electron-hole recombination, low mobility of charge carriers and relatively low quantum efficiency [4–6, 10]. Further improve the photocatalytic activity of Bi_2WO_6 by coupling with other semiconductors can be adopted to promote the separation of photoinduced charge carriers and to enhance the photocatalytic properties [4, 11, 12].

In recent years, silver vanadate (Ag_3VO_4) as n-type semiconductor with narrow band gap has been used to improve the decomposition of pollutants and water splitting under visible light irradiation [13–15]. For example, Zou et al. succeeded in synthesizing of $\text{Ag}_3\text{VO}_4/\text{TiO}_2$ nanorod photocatalyst by a simple sol–gel method and hydrothermal method [16]. The results showed the degradation of toluene of about 70% under visible light within 4 h due to its strong absorption in visible light region and excellent charge separation characteristics. Zhang and Ma succeeded in preparing of $\text{Ag}_3\text{VO}_4/\text{BiOBr}$ n–p heterojunction via chemical deposition for visible-light-driven degradation of rhodamine B (RhB), methylene blue (MB), methyl orange (MO) and tetracycline hydrochloride (TC) [17].

The heterostructure $\text{Ag}_3\text{VO}_4/\text{Bi}_2\text{WO}_6$ nanocomposites with different weight contents of Ag_3VO_4 were prepared by a deposition-precipitation method. The phase and morphology of pure Bi_2WO_6 sample and heterostructure $\text{Ag}_3\text{VO}_4/\text{Bi}_2\text{WO}_6$ nanocomposites were characterized by X-ray diffraction (XRD), scanning electron microscopy (SEM), transmission electron microscopy (TEM), high resolution transmission electron microscopy (HRTEM) and selected area electron diffraction (SAED). The photocatalytic performance of pure Bi_2WO_6 sample and heterostructure $\text{Ag}_3\text{VO}_4/\text{Bi}_2\text{WO}_6$ nanocomposites was investigated through photodegradation of RhB under visible light irradiation. The photocatalytic mechanism of heterostructure $\text{Ag}_3\text{VO}_4/\text{Bi}_2\text{WO}_6$ nanocomposites was also discussed according to the experimental results.

2. Experiment

In a typical synthesis, 0.005 mole $\text{Na}_2\text{WO}_4 \cdot 2\text{H}_2\text{O}$ was dissolved in 100 ml reverse osmosis (RO) water with continuous stirring at room temperature for 30 min, and followed by 0.01 mole $\text{Bi}(\text{NO}_3)_3 \cdot 6\text{H}_2\text{O}$ adding. The final mixture was stirred for at least 30 min. Subsequently, 3 M NaOH was added to the mixture until achieving at the desired pH of 10. The solution mixture was transferred to a 200 ml Teflon-lined autoclave and heated at 180 °C for 20 h. The resulting suspension was left to naturally cool down to room temperature. Following the centrifugation, the obtained precipitates were washed with absolute ethanol and distilled water several times, and dried in an oven at 60 °C for 12 h.

To synthesize Ag_3VO_4 nanoparticles with different weight contents deposited on Bi_2WO_6 nanoplates, 0–10 % of AgNO_3 and Na_3VO_4 by weight, and 2.5 g Bi_2WO_6 sample were dissolved in 100 ml RO water under magnetic stirring for 24 h. The obtained products were separated by filtering, washed by absolute ethanol and dried at 80 °C in an electric oven for 24 h.

XRD patterns of the products were recorded on a Philips X'Pert MPD X-ray diffractometer equipped with Cu K_α radiation ranging from 20° to 80° at a scanning rate of 0.02 deg/s. SEM and TEM images were taken by a scanning electron microscope (JEOL JSM 6335F) with an acceleration voltage of 20 kV and a transmission electron microscope (JEOL JEM 2010) with an acceleration voltage of 200 kV.

The photocatalytic activities of as-synthesized samples were evaluated via photodegradation of RhB solution under visible light irradiation. 200 mg photocatalyst was suspended in 200 ml 10^{-5} M RhB solution each. The suspension was stirred in the dark for 30 min and irradiated by visible light for different lengths of time. The RhB concentration was measured by a UV-visible spectrophotometer (Lambda 25 spectrometer, Perkin Elmer) at λ_{max} of RhB = 554 nm. The decolorization efficiency was calculated by the following equation.

$$\text{Decolorization efficiency (\%)} = \frac{C_0 - C_t}{C_0} \times 100 \quad (1)$$

where C_0 is the initial concentration of RhB and C_t is the concentration of RhB after light irradiation for a period of time (t).

3. Results and discussion

XRD patterns of pure Bi_2WO_6 sample and heterostructure 10 wt% $\text{Ag}_3\text{VO}_4/\text{Bi}_2\text{WO}_6$ nanocomposites are shown in Fig. 1. The XRD pattern of pure Bi_2WO_6 sample can be indexed to pure orthorhombic Bi_2WO_6 phase (JCPDS No. 39-0256 [18]). No impurities such as Bi_2O_3 , WO_3 , etc were detected, indicating that the Bi_2WO_6 phase is highly pure. The XRD pattern of heterostructure $\text{Ag}_3\text{VO}_4/\text{Bi}_2\text{WO}_6$ nanocomposites can be identified to the mixture of Ag_3VO_4 as minor phase and Bi_2WO_6 as major phase. Additional characteristic diffraction of orthorhombic Ag_3VO_4 phase (JCPDS No. 43-0543 [18]) were detected in heterostructure 10 wt% $\text{Ag}_3\text{VO}_4/\text{Bi}_2\text{WO}_6$ nanocomposites at $2\theta = 31.30^\circ$ and 36.11° which correspond to the (121) and (311) planes of Ag_3VO_4 phase. The diffraction peaks of Bi_2WO_6 in heterostructure $\text{Ag}_3\text{VO}_4/\text{Bi}_2\text{WO}_6$ nanocomposites were not shifted as compared to those of pure Bi_2WO_6 phase, indicating that the Ag_3VO_4 phase did not change the bulk Bi_2WO_6 sample. The XRD result certifies that heterostructure $\text{Ag}_3\text{VO}_4/\text{Bi}_2\text{WO}_6$ nanocomposites were synthesized by precipitation-deposition method.

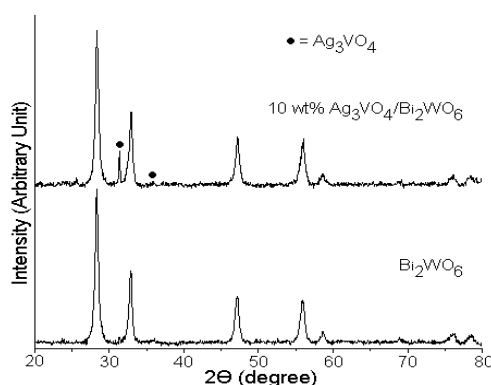


Fig. 1. XRD patterns of pure Bi_2WO_6 sample and heterostructure 10 wt% $\text{Ag}_3\text{VO}_4/\text{Bi}_2\text{WO}_6$ nanocomposites.

Fig. 2 shows low and high magnification SEM images of pure Bi_2WO_6 sample and heterostructure 10 wt% $\text{Ag}_3\text{VO}_4/\text{Bi}_2\text{WO}_6$ nanocomposites. The low magnification SEM image of pure Bi_2WO_6 sample as shown in Fig. 2a presents the morphology of pure Bi_2WO_6 sample composed of uniform square thick nanoplates. The square thick Bi_2WO_6 nanoplates are around 100–150 nm in edge length and 20 nm thick at high magnification SEM image as shown in Fig. 2b. The surface of square thick Bi_2WO_6 nanoplates is very smooth. The SEM image of heterostructure 10 wt% $\text{Ag}_3\text{VO}_4/\text{Bi}_2\text{WO}_6$ nanocomposites at low magnification (Fig. 2c) appears as thick Bi_2WO_6 nanoplates with rough surface. For high magnification image (Fig. 2d), the spherical Ag_3VO_4 nanoparticles supported on the surface of thick Bi_2WO_6 nanoplates were detected, indicating that the Ag_3VO_4 nanoparticles were successfully deposited on the surface of thick Bi_2WO_6 nanoplates by forming heterostructure $\text{Ag}_3\text{VO}_4/\text{Bi}_2\text{WO}_6$ nanocomposites.

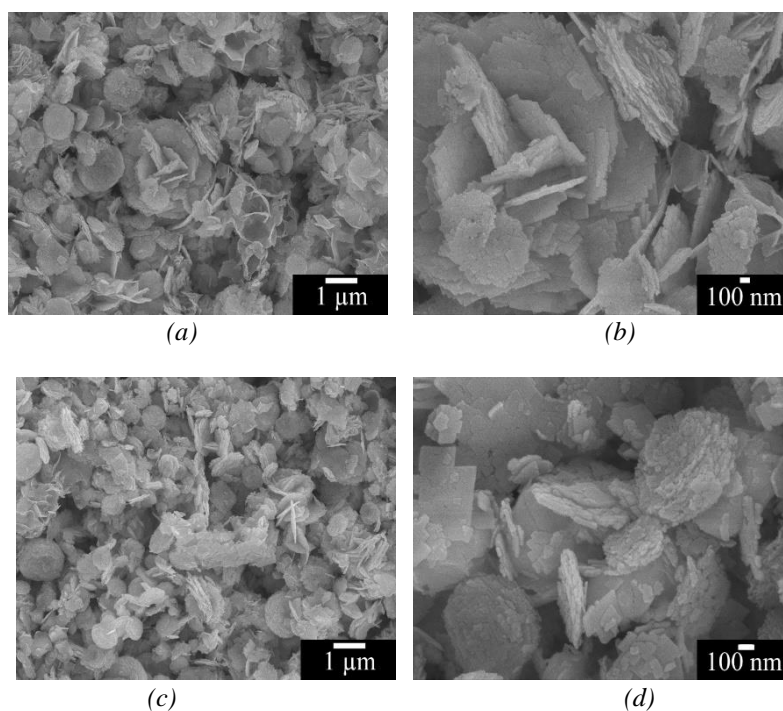


Fig. 2. Low and high magnification SEM images of (a and b) pure Bi_2WO_6 sample and (c and d) heterostructure $10\ \text{wt}\% \text{Ag}_3\text{VO}_4/\text{Bi}_2\text{WO}_6$ nanocomposites.

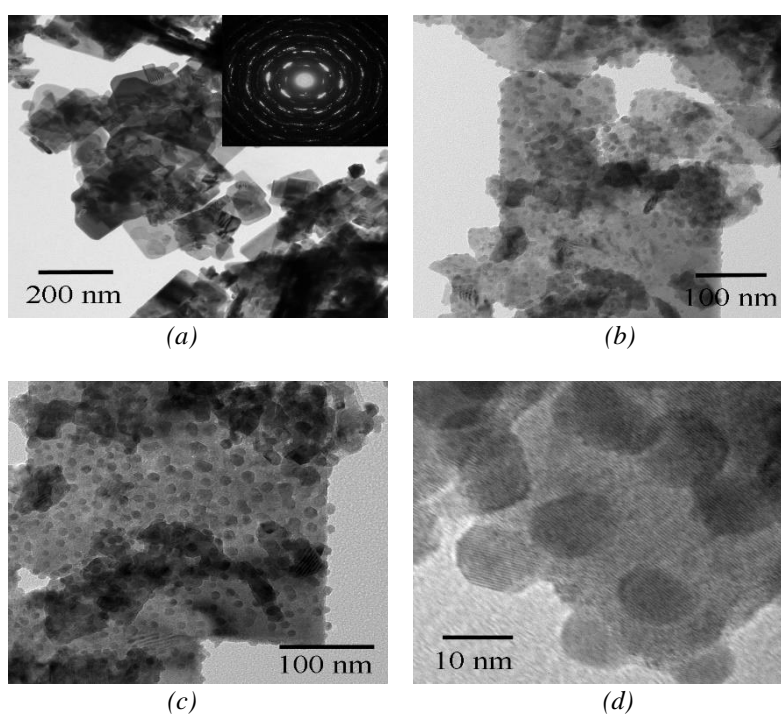


Fig. 3. TEM, SAED and HRTEM results of (a) pure Bi_2WO_6 sample and (b–d) $10\ \text{wt}\% \text{Ag}_3\text{VO}_4/\text{Bi}_2\text{WO}_6$ nanocomposites.

Fig. 3 shows the TEM, SAED and HRTEM results of pure Bi_2WO_6 sample and heterostructure $\text{Ag}_3\text{VO}_4/\text{Bi}_2\text{WO}_6$ nanocomposites. The TEM image of as-synthesized Bi_2WO_6 sample (Fig. 3a) shows uniform thick Bi_2WO_6 nanoplates. The SAED pattern of the as-synthesized

Bi_2WO_6 nanoplates as inserted in Fig. 3a can be indexed to the (311), (060), (200) and (002) planes of orthorhombic Bi_2WO_6 phase. TEM image of heterostructure 10 wt% $\text{Ag}_3\text{VO}_4/\text{Bi}_2\text{WO}_6$ nanocomposites at low magnification (Fig. 3b) appears as uniformly distributed Ag_3VO_4 nanoparticles with particles size of 10–12 nm supported on the surface of thick Bi_2WO_6 nanoplates. It can be seen that the fully Ag_3VO_4 nanoparticles were deposited on the surface of thick Bi_2WO_6 nanoplates as shown in Fig. 3c. The clear (121) crystalline plane of Ag_3VO_4 phase was observed by HRTEM analysis as shown in Fig. 3d, indicating the formation of heterojunction of Ag_3VO_4 nanoparticles and Bi_2WO_6 nanoplates. The photocatalytic properties were enhanced because of the separation of photo-excited charge carriers and the inhibition of photo-induced electron–hole pairs [1, 11, 12, 14, 17].

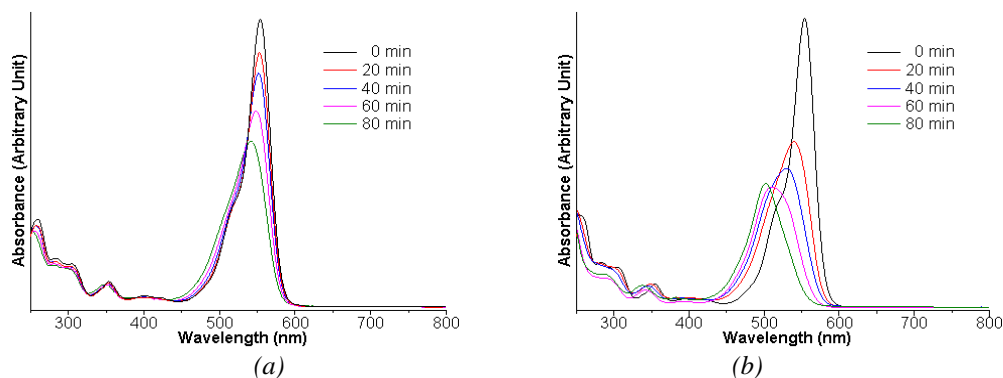


Fig. 4. Temporal UV–visible absorption for photocatalytic degradation of RhB under visible light irradiation in the presence of pure Bi_2WO_6 sample and heterostructure 10 wt% $\text{Ag}_3\text{VO}_4/\text{Bi}_2\text{WO}_6$ nanocomposites.

In the photocatalytic experiment, photocatalytic degradation of RhB in the presence of pure Bi_2WO_6 sample and heterostructure $\text{Ag}_3\text{VO}_4/\text{Bi}_2\text{WO}_6$ nanocomposites as photocatalysts was evaluated under visible light irradiation from a Xe lamp ($\lambda \geq 420$ nm). Fig. 4 shows the temporal UV–visible absorption spectra for photocatalytic degradation of RhB under visible light irradiation in the presence of pure Bi_2WO_6 sample and heterostructure 10 wt% $\text{Ag}_3\text{VO}_4/\text{Bi}_2\text{WO}_6$ nanocomposites. The intensity of characteristic absorption peak of RhB over heterostructure 10 wt% $\text{Ag}_3\text{VO}_4/\text{Bi}_2\text{WO}_6$ nanocomposites shows a quick decrease while the intensity of the RhB over pure Bi_2WO_6 sample decreased slightly even at same condition. The results indicate that RhB over heterostructure 10 wt% $\text{Ag}_3\text{VO}_4/\text{Bi}_2\text{WO}_6$ nanocomposites was degraded faster than that over pure Bi_2WO_6 sample. It can be seen that the maximum absorption peak of RhB at 554 nm decreased gradually as the prolonging exposure visible light irradiation time. Within 80 min, the characteristic absorption peak of RhB over heterostructure 10 wt% $\text{Ag}_3\text{VO}_4/\text{Bi}_2\text{WO}_6$ nanocomposites gradually shows blue-shift in a step-by-step manner to 498 nm by N-deethylation of RhB under visible light irradiation [9, 11, 12]. It is well known that RhB is N,N,N',N' -tetraethyl rhodamine, its λ_{max} of UV–visible spectrum is 554 nm. The N-deethylation of RhB contains N,N,N' -triethyl rhodamine ($\lambda_{\text{max}} = 539$ nm), N,N' -diethyl rhodamine ($\lambda_{\text{max}} = 522$ nm), N-ethyl rhodamine ($\lambda_{\text{max}} = 510$ nm) and rhodamine ($\lambda_{\text{max}} = 498$ nm) [19–21].

Fig. 5a shows the relative concentration of RhB remaining in the solution as a function of irradiation time over pure Bi_2WO_6 sample and heterostructure $\text{Ag}_3\text{VO}_4/\text{Bi}_2\text{WO}_6$ nanocomposites under visible light irradiation. The results indicate that heterostructure 10 wt% $\text{Ag}_3\text{VO}_4/\text{Bi}_2\text{WO}_6$ nanocomposites exhibit the highest photocatalytic performance of 95% for RhB degradation within 80 min under visible light irradiation while the photocatalytic degradation of RhB over pure Bi_2WO_6 sample is only 52.45% within 80 min under visible light irradiation. The enhanced photocatalytic activity of heterostructure $\text{Ag}_3\text{VO}_4/\text{Bi}_2\text{WO}_6$ nanocomposites is probably relevant to the lowest recombination rate of electrons and holes by synergistic effect [22, 23]. The photodegradation of RhB over pure Bi_2WO_6 sample and heterostructure $\text{Ag}_3\text{VO}_4/\text{Bi}_2\text{WO}_6$ nanocomposites under visible light irradiation was fitted well with a pseudo-first-order kinetic

model as shown in Fig. 5b [2, 10, 11, 12]. The kinetic rate constant for photodegradation of RhB over heterostructure 0 wt%, 1 wt%, 5 wt% and 10 wt% $\text{Ag}_3\text{VO}_4/\text{Bi}_2\text{WO}_6$ nanocomposites are $7.99 \times 10^{-3} \text{ min}^{-1}$, 0.0164 min^{-1} , 0.0233 min^{-1} and 0.0349 min^{-1} , respectively. The heterostructure 10 wt% $\text{Ag}_3\text{VO}_4/\text{Bi}_2\text{WO}_6$ nanocomposites reached 4.37 times of pure Bi_2WO_6 sample, indicating that the photocatalytic performance of Bi_2WO_6 was significantly improved by forming heterostructure $\text{Ag}_3\text{VO}_4/\text{Bi}_2\text{WO}_6$ nanocomposites [1, 11, 12, 19].

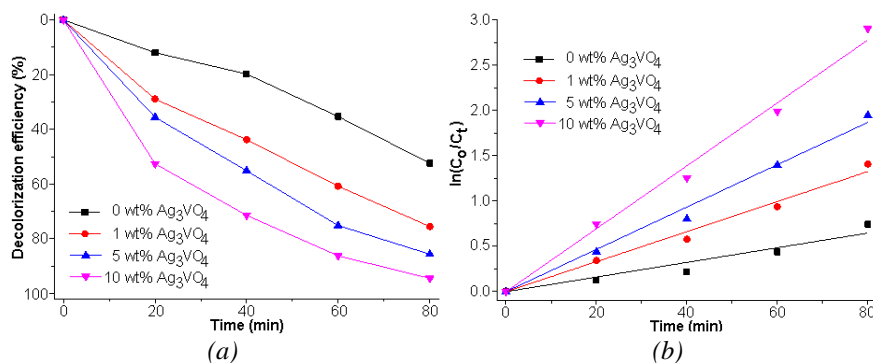


Fig. 5. (a) Decolorization efficiency and (b) pseudo-first-order plot of the photocatalytic degradation of RhB by the $\text{Ag}_3\text{VO}_4/\text{Bi}_2\text{WO}_6$ nanocomposites with different Ag_3VO_4 contents under visible light irradiation.

In addition, the photostability of the re-used heterostructure 10 wt% $\text{Ag}_3\text{VO}_4/\text{Bi}_2\text{WO}_6$ nanocomposites was investigated through RhB degradation for five cycles to evaluate the practical application as shown in Fig. 6. The photocatalytic RhB degradation of heterostructure 10 wt% $\text{Ag}_3\text{VO}_4/\text{Bi}_2\text{WO}_6$ nanocomposites was approximately 92.59% after five recycles, indicating that the heterostructure 10 wt% $\text{Ag}_3\text{VO}_4/\text{Bi}_2\text{WO}_6$ nanocomposites is excellent stability and reusability.

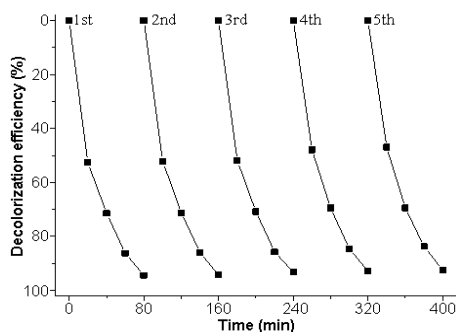


Fig. 6. Stability of the heterostructure 10 wt% $\text{Ag}_3\text{VO}_4/\text{Bi}_2\text{WO}_6$ nanocomposites for RhB degradation.

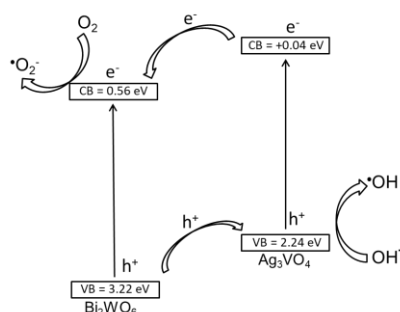


Fig. 7. Schematic energy band diagram of the heterostructure $\text{Ag}_3\text{VO}_4/\text{Bi}_2\text{WO}_6$ nanocomposites.

A possible photodegradation mechanism of RhB by $\text{Ag}_3\text{VO}_4/\text{Bi}_2\text{WO}_6$ nanocomposites can be depicted by a schematic energy band diagram of the composites as shown in Fig. 7. The VB (+3.22 eV) and CB (+0.56 eV) edges of Bi_2WO_6 are more positive than the VB (+2.24 eV) and CB (+0.04 eV) edges of Ag_3VO_4 [1, 10, 12]. Under visible light irradiation, the photo-induced electrons and holes were excited to CB of both Bi_2WO_6 and Ag_3VO_4 semiconductors. Concurrently, the photo-induced holes on VB of Bi_2WO_6 easily flow to VB of Ag_3VO_4 through the interface which can decrease the recombination rate of electrons and holes [1, 3, 11, 12]. The generated active $\cdot\text{O}_2^-$ and $\cdot\text{OH}$ radicals degraded the RhB organic dye by transforming the dye into H_2O and CO_2 [1, 4, 11, 12]. Thus the heterostructure $\text{Ag}_3\text{VO}_4/\text{Bi}_2\text{WO}_6$ nanocomposites exhibited photocatalytic performance more than the pure Bi_2WO_6 sample.

4. Conclusions

Heterostructure $\text{Ag}_3\text{VO}_4/\text{Bi}_2\text{WO}_6$ nanocomposites were successfully synthesized by a deposition-precipitation method. The analytical results show good distribution of Ag_3VO_4 nanoparticles supported on Bi_2WO_6 nanoplates. The 10 wt% $\text{Ag}_3\text{VO}_4/\text{Bi}_2\text{WO}_6$ nanocomposites showed the highest photocatalytic activity for degradation of RhB under visible light irradiation. These results certify that heterostructure $\text{Ag}_3\text{VO}_4/\text{Bi}_2\text{WO}_6$ nanocomposites are an effective photocatalyst under visible light irradiation and have a promising potential application for the removal of organic pollutants.

Acknowledgement

We are extremely grateful to Prince of Songkla University, Hat Yai, Songkhla 90112, Thailand for providing financial support the research.

References

- [1] B. Chen, Y. Deng, H. Tong, J. Ma, *Superlatt. Microstr.* **69**, 194 (2014).
- [2] M. H. Selvia, P. R. Vangab, M. Ashok, *Optik* **173**, 227 (2018).
- [3] K. Zhang, J. Wang, W. Jiang, W. Yao, H. Yang, Y. Zhu, *Appl. Catal. B* **232**, 175 (2018).
- [4] L. Wange, G. Yang, D. Wang, C. Lu, W. Guan, Y. Li, J. Deng, J. Crittenden, *Appl. Surf. Sci.* **495**, 143521 (2019).
- [5] Q. Zhang, M. Wang, M. Ao, Y. Luo, A. Zhang, L. Zhao, L. Yan, F. Deng, X. Luo, *J. Alloy. Compd.* **805**, 41 (2019).
- [6] W. Huo, W. Xu, T. Cao, X. Liu, Y. Zhang, F. Dong, *Appl. Catal. B* **254**, 206 (2019).
- [7] J. Li, Z. Liang, Q. Song, X. Xu, *Appl. Surf. Sci.* **478** (2019).
- [8] M. Arif, M. Zhang, J. Yao, H. Yin, P. Li, I. Hussain, X. Liu, *J. Alloy. Compd.* **792**, 878 (2019).
- [9] X. Wang, L. Chang, J. Wang, N. Song, H. Liu, X. Wan, *Appl. Surf. Sci.* **270**, 685 (2013).
- [10] L. Guo, Q. Zhao, C. Wang, H. Shen, X. Han, K. Zhang, D. Wang, F. Fu, *Mater. Res. Bull.* **118**, 110520 (2019).
- [11] S. Jonjana, A. Phuruangrat, T. Thongtem, B. Kuntalue, S. Thongtem, *Mater. Lett.* **218**, 146 (2018).
- [12] S. Jonjana, A. Phuruangrat, S. Thongtem, O. Wiranwetchayan, T. Thongtem, *Mater. Lett.* **180**, 93 (2016).
- [13] S. Z. Wu, K. Li, W. D. Zhang, *Appl. Surf. Sci.* **324**, 324 (2015).
- [14] P. Wang, H. Tang, Y. Ao, C. Wang, J. Hou, J. Qian, Y. Li, *J. Alloy. Compd.* **688**, 1 (2016).
- [15] P. Raizada, A. Sudhaik, P. Singh, P. Shandilya, A. K. Saini, V. K. Gupta, J. H. Lim, H. Jung, A. Hosseini-Bandegharai, *Sep. Purif. Technol.* **212**, 887 (2019).
- [16] X. Zou, Y. Dong, X. Zhang, Y. Cui, *Appl. Surf. Sci.* **366**, 173 (2016).
- [17] J. Zhang, Z. Ma, *Mole. Catal.* **436**, 190 (2017).

- [18] Powder Diffract. File, JCPDS-ICDD, 12 Campus Boulevard, Newtown Square, PA 19073-3273, U.S.A., (2001).
- [19] X. Hao, J. Zhao, Y. Zhao, D. Ma, Y. Lu, J. Guo, Q. Zeng, *Chem. Eng. J.* **229**, 134 (2013).
- [20] S. Jonjana, A. Phuruangrat, S. Thongtem, T. Thongtem, *Mater. Lett.* **216**, 92 (2018).
- [21] A. Phuruangrat, A. Maneechote, P. Dumrongrojthanath, N. Ekthammathat, S. Thongtem, T. Thongtem, *Superlatt. Microstr.* **78**, 106 (2015).
- [22] N. Güy, M. Özacar, *J. Photochem. Photobio. A* **370**, 1 (2019).
- [23] M. Kuang, J. Zhang, W. Wang, J. Chen, R. Liu, S. Xie, J. Wang, Z. Ji, *Solid State Sci.* **96**, 105901 (2019).